

Investigation of alkaline earth element substituted Lanthanum Ferrite nanoparticles and its characterization

S. Saseetha^{a,b,*}, M. Nagarajan^a, S. Subha^a, K. A. Rani^b, S. C. Vella Durai^c

^aResearch Department of Physics, V.O.Chidambaram College, Thoothukudi-628008, Tamilnadu, India

^bDepartment of Physics, SSDM College, Kovilpatti-628501, Tamil Nadu, India.

^cPG and Research Department of Physics, Sri Paramakalyani College, Alwarkurichi, Tenkasi-627412, Tamil Nadu, India (Affiliated to Manonmanium Sundaranar University, Tirunelveli - 627018)

Pure Lanthanum Ferrite (LaFeO₃) nanoparticles and Lanthanum Magnesium Ferrite (LaMg_xFe_{1-x}O₃) nanocomposites have been prepared by the sol-gel auto-combustion method. The structural and morphological properties were investigated by X-ray diffraction (XRD), Scanning electron microscopy (SEM) and energy dispersive X-ray (EDAX) spectroscopy. Powder XRD studies revealed that the samples are pure orthorhombic perovskite crystals with a size of around 20–50 nm. The FT-IR spectra of pure and composites was confirmed the formation perovskite structure. It has been discovered that composites material functions as an electrode in supercapacitors after its electrical characteristics have been examined by galvanostatic charging and discharging (GCD), cyclic voltammetry (CV), and electrochemical impedance spectroscopy (EIS) with a 2 M KOH electrolyte.

(Received October 2, 2023; Accepted January 5, 2024)

Keywords: Auto-combustion, Bandgap, Electrode, Lanthanum, Perovskite, Supercapacitor

1. Introduction

Lanthanum iron oxide (LaFeO₃) is an iron oxide [1] that can be very well used in fields such as electricity and many other industries due to its unique properties. Nanoscience helps us change the properties of metal oxides to obtain new structures, electrical and electronic energy [2]. Changing the size of nanoparticles creates new materials ranging from less than 100 nanometers in a single dimension. There is a difference in terms of applications and properties of LaFeO₃ nanoparticles are reviewed [3]. Different preparation methods such as precipitation method and sol-gel automatic combustion method are being studied to increase quality and efficiency. At various nanoscales, LaFeO₃ exists in different sizes of 1D (such as rods), 2D (such as plates) and 3D structures (such as flowers), so it has received many applications as new products [4]. Similarly, metal-doped LaFeO₃ nanoparticles also obtained properties and behavior [5]. Doped LaFeO₃ has a chorus-like morphology with a structure consisting of several ordered phases [6]. Photocatalytic, battery, sensor and electrical properties of LaFeO₃ nanoparticles and their doping with different elements were investigated [7]. Thanks to the use of all the benefits of LaFeO₃ nanoparticles in the platform, new analyzes of LaFeO₃ nanoparticles are also possible. Additionally, identification of new metals in aqueous solutions may be a solution for better removal of contaminants [8]. The use of LaFeO₃ nanoparticles and their doping with earth metals has also begun to be used in many applications. Although the problems related to LaFeO₃ have been investigated, its effect on the properties of the material has not been investigated much. As mentioned in [9], different additives were investigated for LaFeO₃.

* Corresponding author: sasiathil@gmail.com
<https://doi.org/10.15251/JOR.2024.201.35>

Since ferrite material is used in several technologies, including photo catalysts, magnetic properties and sensors for sensing gases, it has undergone a great deal of study [10]. A relatively small quantity of rare earth metals can be utilized to alter the characteristics of ferrites. Several recent investigations have explained that the intrinsic studies of ferrites can be enhanced by incorporating rare earth ions [11–13]. The chemical formula of such ferrite is ABO_3 , where A stands for rare earth elements and B stands for transition metals. One of the oxides in the perovskite class is $LaFeO_3$. $LaFeO_3$ has an orthorhombic or cubic crystal structure with band gap energy of 2.1 eV. [14] The particle size, surface morphology, thermal, and electrical properties of $LaFeO_3$ are modified by the inclusion of transition metal [15]. To emphasise the characteristics of ferrites, several attempts have been made by incorporating magnetic and nonmagnetic materials with different sites A and B of perovskite materials like lanthanum [16], manganese [17], neodymium [18], praseodymium [19], zinc [20], etc. Lanthanide and actinides are well-known rare earth elements. In the Lanthanide series, lanthanum is the lightest, most abundant material, having the lowest vapour pressure at its melting point, the highest boiling point, and a superconducting nature at atmospheric pressure. [21]. By the method of sol-gel citrate combustion, ferrites of rare earth element nanowires with anodic aluminium oxide were synthesised (22). The addition of catalysts to the various preparation routes has previously been investigated [23, 24], and the morphological features of electrodes were compared. This investigation explicates the preparation of Mg substitution of lanthanum ferrite nanoparticles by citrate autocombustion route.

2. Experimental details

2.1. Materials

All chemicals ($La(NO_3)_3 \cdot 9H_2O$, $Mg(NO_3)_2 \cdot 6H_2O$, $Fe(NO_3)_3 \cdot 9H_2O$, and citric acid) were purchased (up to 98.99% purity) from Aldrich and Rankem chemical suppliers and used as received. The de-ionized water was used as the solvents. The entire chemical was used without any further purification.

2.2. Preparation of $LaFeO_3$ nanoparticles and $LaMgFeO_3$ nanocomposites

$La(NO_3)_3 \cdot 9H_2O$, $Mg(NO_3)_2 \cdot 6H_2O$, $Fe(NO_3)_3 \cdot 9H_2O$, and citric acid were used as starting materials for the sol-gel citrate self-ignition technique to synthesize with mol of ($x = 0.0, 0.1, 0.2,$ and 0.3). The metal nitrates were dissolved in citric acid at $50^\circ C$, and sol was formed with continuous stirring for 3 hours. Next, the sol gets dehydrated at $120^\circ C$ for two hours so as to form a gel. The ash-like powder is then formed, followed by autocombustion. This ash was taken in a silica crucible and fine-powdered by grinding. In order to produce magnesium-doped lanthanum ferrite (LFM) nanoparticles, the fine powder must be calcined for duration of five hours at $650^\circ C$ in the muffle furnace.

2.3. Material characterizations

X-ray diffraction pattern for the $LaFeO_3$ nanoparticles and $LaMgFeO_3$ nanocomposites was analyzed using an X-ray diffractometer (X'Pert Pro - PANalytic) using $Cu K_\alpha$ radiation of wavelength $\lambda=0.1541$ nm in the scan range $2\theta=10-80^\circ$. Morphology of the nanoparticles was analyzed using scanning electron microscope (DESKTOP Mini - SEM with EDS, SNE- 3200M, SEC) which also has been used for compositional analysis of the prepared nanoparticles. The optical absorption spectra of prepared nanoparticles were recorded using a UV-VIS spectrophotometer (Thermofisher Evaluation 220). The functional groups of prepared nanoparticles were recorded using a FTIR spectrophotometer (Thermo Nicolet 380). The electrochemical capacitive behavior has been examined using a (CH – Instrument) electrochemical work station.

3. Results and discussion

3.1. Powder XRD Studies

Figure 1 show XRD spectrum for pure LaFeO_3 , nanoparticles and Mg doped LaFeO_3 nanocomposite with different concentration. It can be clearly seen that, there is no difference in XRD patterns of pure LaFeO_3 , nanoparticles and LaMgFeO_3 nanocomposite. The XRD spectrum of LaMgFeO_3 nanocomposite consists of peaks corresponding to the presence of LaFeO_3 , nanoparticles used during the synthesis. The absence of other overlapping peaks at the sample peak position indicates that the sample preparation was single-phase, i.e. only pure LaFeO_3 molecules were present.

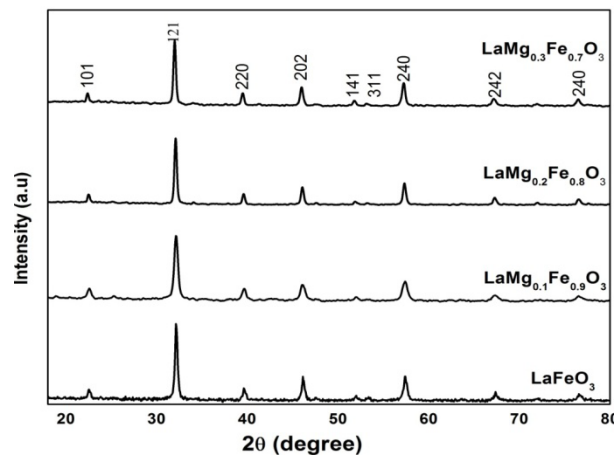


Fig. 1. XRD spectra of LaFeO_3 nanoparticles and LaMgFeO_3 nanocomposites.

LaFeO_3 crystalline sizes were estimated using XRD analysis. Scherer's equation has been applied to determine the perovskite phases of lanthanum ferrite.

$$D = \frac{k\lambda}{\beta_{hkl} \cos\theta} \quad (1)$$

Here, D is the crystalline size associated with the crystal in nanometers, k is the Scherer constant (0.89), λ is the X-ray wavelength (1.54\AA), θ is the Bragg's angle associated with the primary peak of (121) higher intensity, and β_{hkl} is the (FWHM) full width at half maximum in radians. The average crystallite size is found to be 20 nm for LaFeO_3 , and the average values of the LaMgFeO_3 compound are found to be 30 nm. According to a powder diffraction file (JCPDS card no. 37-1493), the samples showed a pure orthorhombic perovskite structure having strong and narrow phase peaks, as was previously described [25].

3.2. FTIR studies

Figure 2 shows an FTIR spectrum was performed to examine the functional group of LaFeO_3 nanoparticles and LaMgFeO_3 nanocomposites in the wave number range of 4000 to 400 cm^{-1} with an orthorhombic perovskite structure. FT-IR spectra of LaFeO_3 were recorded to investigate the chemical bonding between Fe-O atoms in mono-structured LF. The formation of a typical perovskite structure is made clear by the mode of metal-oxygen bond vibration that ranges from 400 to 600 cm^{-1} . [26]. With rare earth and transition metal ions residing in the A site and B site of the compound (ABO_3), a kind of perovskite structure, the Fe-O stretching vibration band can occur at 555 cm^{-1} . A peak at 1638 cm^{-1} is present, and the H-O stretching mode is responsible for its presence. [27]. The FT-IR spectrum is in good agreement with the XRD pattern of LaFeO_3 nanoparticles and LaMgFeO_3 nanocomposites.

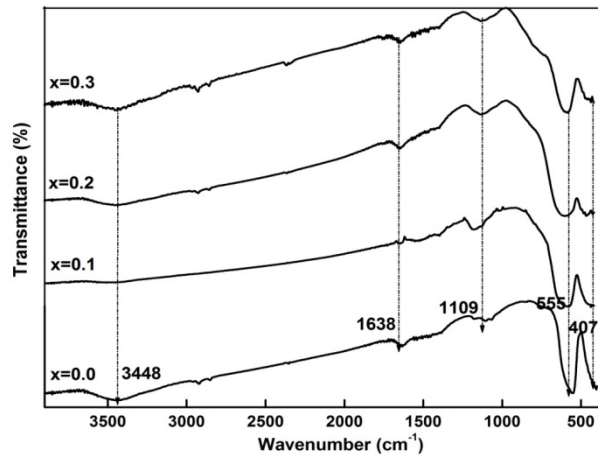


Fig. 2. FT-IR spectra of LaFeO_3 nanoparticles and LaMgFeO_3 nanocomposites.

3.3. UV-Vis Studies

The UV-vis spectrum of $\text{La}_{1-x}\text{Mg}_x\text{FeO}_3$ ($x = 0, 0.1, 0.2,$ and 0.3) nanopowders are shown in Figure 3. In Figures 3 and 4, broad absorption peaks are observed at approximately 405 nm for all the samples. A plot of $(ah\nu)^2$ vs. $h\nu$ is used to calculate band gap energy (E_g) for pure and Mg doped LaFeO_3 nanoparticles, which was observed to be near 2.18 eV with no significant change after doping. It is also witnessed that the gathering of Mg ions causes substantial alterations in the absorption spectrum of LaFeO_3 showing the visible region causing a large absorbance over the entire visible region with elevated Mg concentration. The optical band gaps (E_g) of the samples can be determined, and the obtained values are 2.18 eV, 2.16 eV, 2.14 eV, and 2.18 eV. It is clear that by increasing Mg content, the optical band gap does not vary significantly [28].

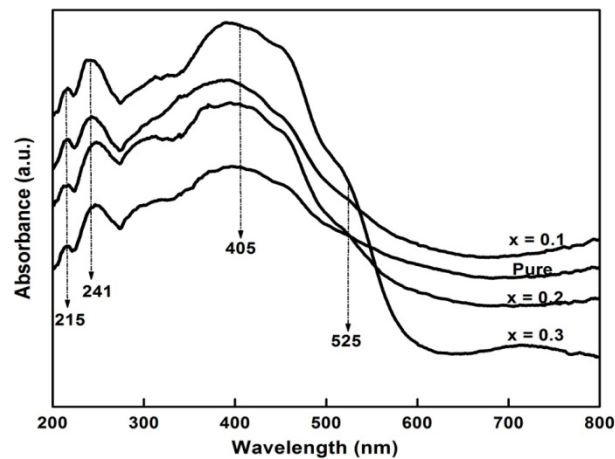


Fig. 3. UV-vis absorption plot of LaFeO_3 nanoparticles and LaMgFeO_3 nanocomposites.

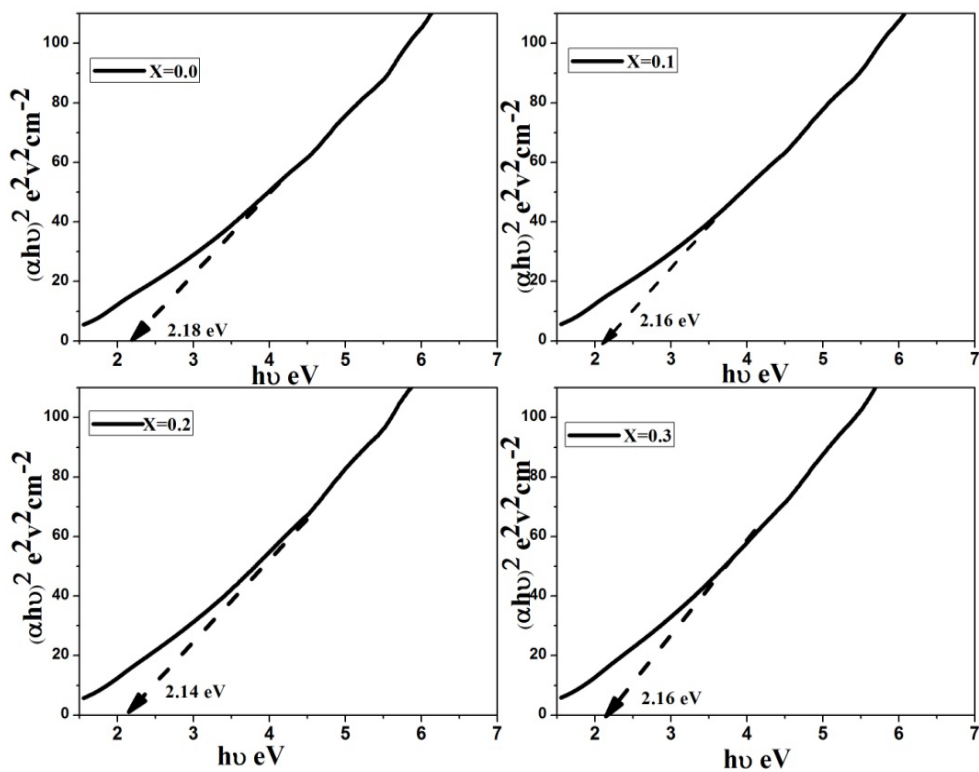


Fig. 4. Tauc's plot of LaFeO_3 nanoparticles and LaMgFeO_3 nanocomposites.

3.4. Morphology studies

The SEM micrographs of the LaFeO_3 and LaMgFeO_3 samples are shown in Figure 5.

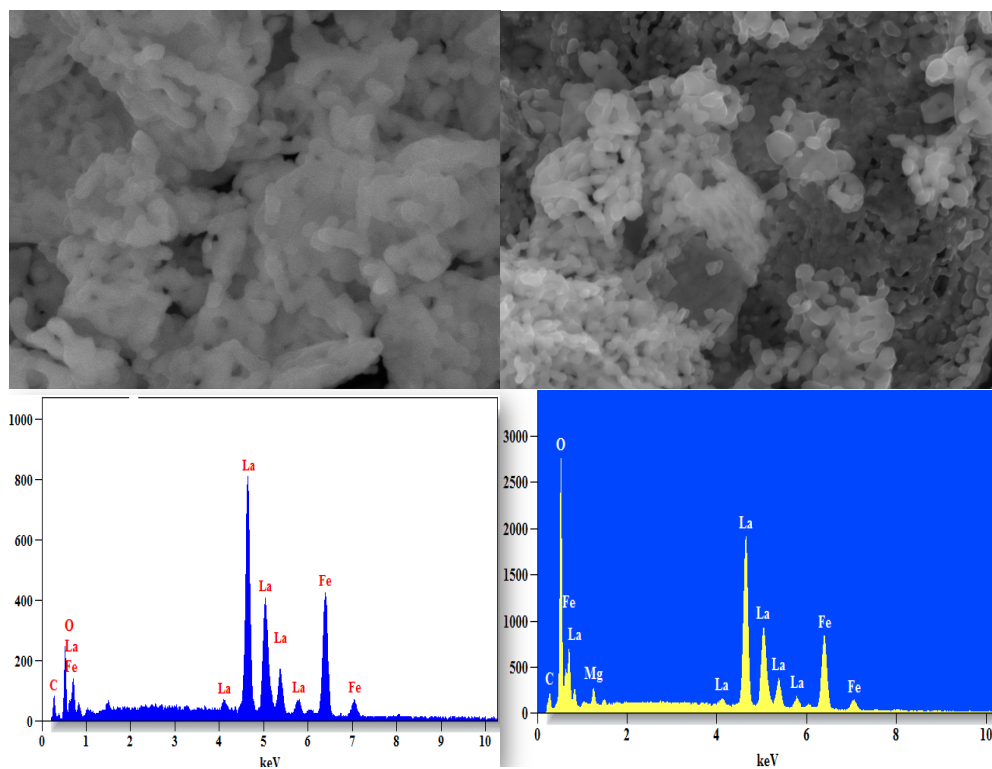


Fig. 5. SEM with edax of LaFeO_3 nanoparticles and LaMgFeO_3 nanocomposites.

The Mg-doped materials had sporadic morphology and were discovered to have agglomerated particles that resembled coral-like structures. The elemental compositions of synthesised ferrite samples are shown in Fig. 5. Elements like La, Fe, O, C, and Mg were identified. The carbon (C) element was present in the EDAX spectrum since carbon tape was used in the EDAX during analysis. No further elements were noted or identified, and it is concluded that the synthesised ferrite samples have no impurities. The observed La, Mg, and Fe percentage values are tabulated inside the EDAX spectrum (Figs. 5). These values are compatible with the precursors of Fe, Mg, and La used in the citrate combustion method.

3.5. The electrochemical studies

The electrochemical capacitive behavior has been examined by the GCD, CV, and EIS tests on the as-fabricated pure LaFeO₃ (LF) and LaMgFeO₃ (LFM) nanocomposites. The measurements for the samples were carried out under normal conditions for electrochemical behaviour, such as electrochemical impedance spectroscopy (EIS), cyclic voltammetry (CV), and galvanostatic charging and discharging (GCD) in a 2 M KOH electrolyte. In the open-circuit potential with a frequency ranging from 100 kHz to 100 MHz, the EIS test was carried out. With a potential window of 0.1–0.6 V, CV investigations have been carried out with various scan rates. The GCD investigations have been implemented at varying current densities from 1 to 5 A/g in a constant potential window rate between 0.1 and 0.5 V. Using Eqs. (1) and (2), it was possible to compute the specific capacitance C_{sp} (F/g) from CV and GCD. [29] and [30, 31], respectively

$$C_{sp} = \int \frac{I \Delta t}{mv \Delta V} \quad (1)$$

$$C_{sp} = \frac{I \Delta t}{m \Delta V} \quad (2)$$

Here I is the current in (A), Δt is the discharging time in (s), m is the mass of active material in (mg), v is the scan rate in (mV/s), and ΔV is the potential window in (V). Fig. 6a shows the CV curves of LFM2 at various scan rates of 10 mV/s to 100 mV/s in the 2M KOH electrolyte, and the range of potential is 0.1V to 0.6V. The area under the CV curve increases gradually with the increase in scan rate. The CV current is proportionate to the scan rate [32]. The specific capacitance was determined, ranging from 10 mV/s to 100 mV/s. The value of specific capacitance is high (323 F/g) at the scan rate of 10 mV/s. The value of specific capacitance is lower (112 F/g) at the scan rate of 100 mV/s. The graph plotted between specific capacitance and scan rate is shown in Fig. 6b. It is reported that the high ohmic resistance occurred at a large scan rate [33, 34]. The comparison between pristine LF and LFM2 particles is shown in figs. 5c and 5d.

The frequency range of 100 kHz to 100 MHz in a 2 M KOH electrolyte with an open circuit voltage has been studied using electrochemical impedance spectroscopy (EIS) analysis of the LFM2 electrode. In the Nyquist graph (Fig. 5e), the solution resistance (R_s) and charge transfer resistance (R_{ct}) have been identified as $R_s = 0.7$ ohm and $R_{ct} = 3.44$ ohm. The image which is inserted in Fig. 6f expresses the equivalent circuit. Fig. 6f represents the Nyquist's plot of the samples LF and LFM2

The specific capacitance C_{sp} (F/g) was estimated from GCD curves at various current densities using Eq. (2). Figs. 6g and 6h demonstrate the variation of specific capacitance values with current density. The comparison of pure LF and doped lanthanum LFM2 can be noted in figs.6i & 6j

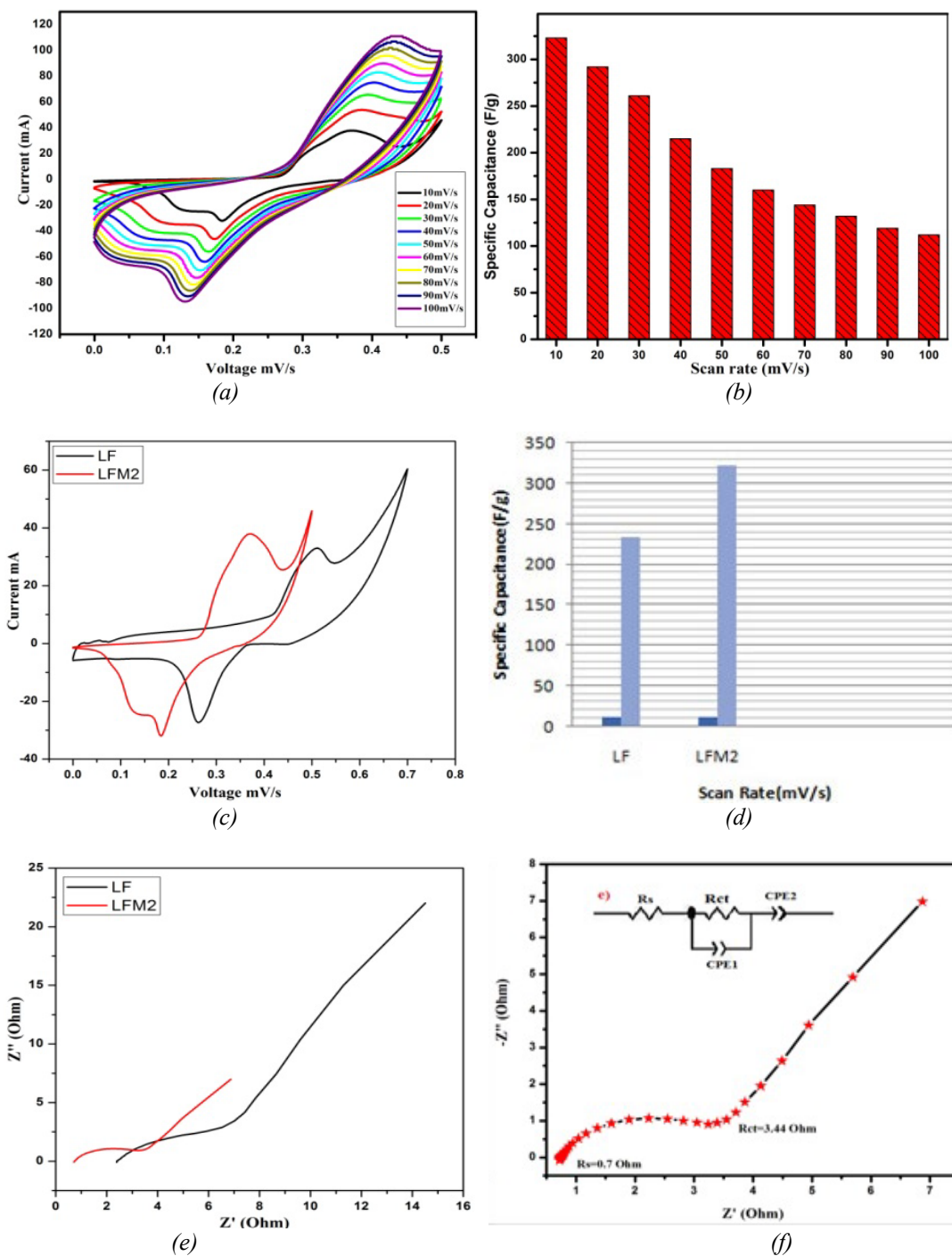


Fig. 6. a) CV Plot (voltage vs current), b) Represents scan rate vs specific capacitance, c) and d) comparison LF and LFM2; e) Nyquist plot, f) Equivalent circuit;

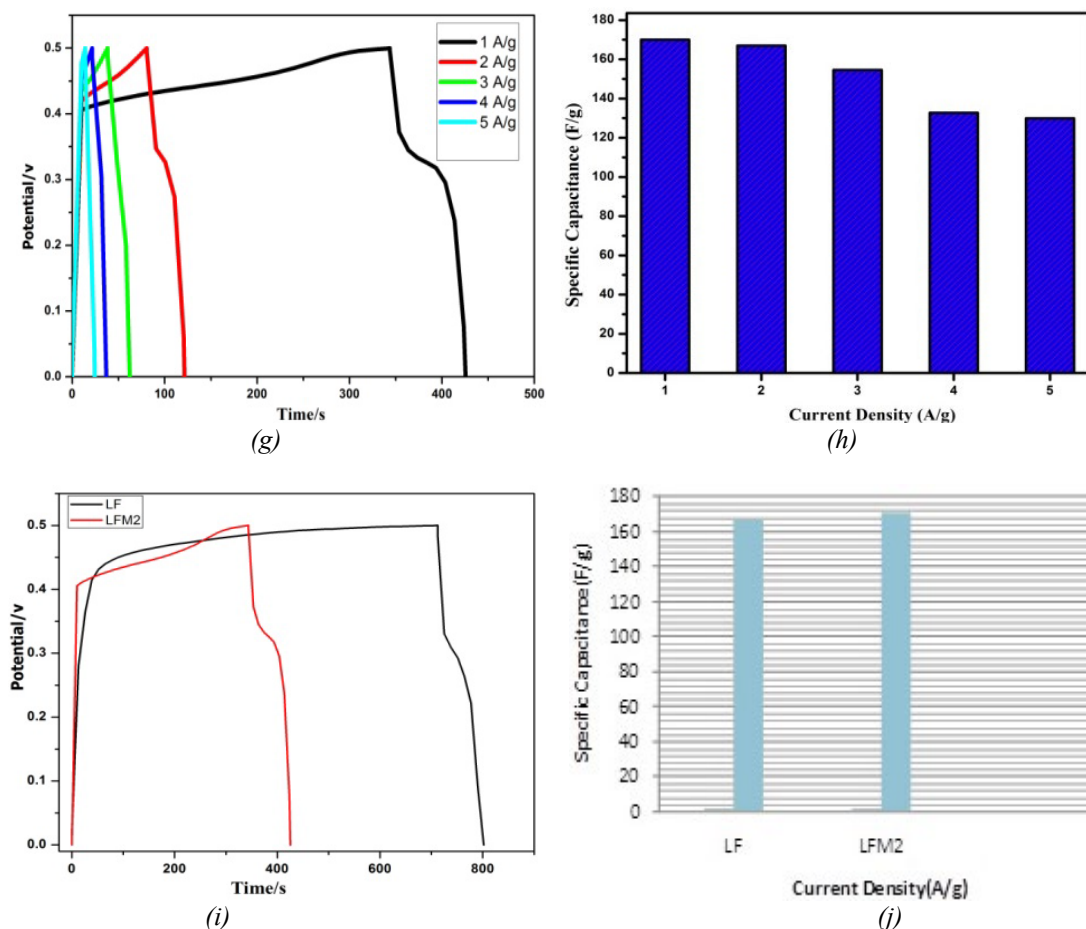


Fig. 6. g) GCD (current densities time vs potential range);
 h) Represents Specific Capacitance Vs Current density; i) and j) comparison of LF & LFM2

4. Conclusion

LaMgFeO₃ nanoparticles were successfully synthesized by the sol-gel citrate autocombustion method. The structural, morphological, and electrochemical properties of the LaMgFeO₃ nanoparticles were examined. The formation of single-phase lanthanum ferritenanoparticles was confirmed by XRD patterns. The formation of porous LFM2 nanoparticles facilitates the electric charge transfer of the electrolyte, which was confirmed by SEM micrographs. The formation of LaMgFeO₃ without any impurities was confirmed by the EDAX spectrum. In a 2 M KOH electrolyte, the LFM2 electrode was investigated using CV, GCD, and EIS. LaMgFeO₃ nanoparticles were synthesised using the sol-gel citrate auto-combustion process, and their electrochemical characteristics exhibited Faradaic behaviour with a specific capacitance of 323 F/g at a slow scan rate of 10 mV/s.

Acknowledgements

I, S. Saseetha (Reg.No: 1922232132014) is thankful to authorities of V. O. Chidambaram College, Thoothukudi and Manonmaniam Sundaranar University, Tirunelveli, Tamilnadu, India for providing necessary research facilities.

References

- [1] M. A. Gabal, F. Al-Solami, Y. M. Al Angari, A. A. Ali, A. A. Al-Juaid, K. Huang, M. Alsabban, *Ceramics International*, 45(13), 16530 (2019); <https://doi.org/10.1016/j.ceramint.2019.05.187>
- [2] R. Jothiramalingam, H. Al-Lohedan, A. Karami, *Journal of Ovonic Research*, 19(5), 525 (2023); <https://doi.org/10.15251/JOR.2023.195.525>
- [3] N. Joudeh, D. Linke, *Journal of Nanobiotechnology*. 262, 20 (2022); <https://doi.org/10.1186/s12951-022-01477-8>
- [4] J. Hornak, *Int. J. Mol. Sci.* 22, 12752 (2021); <https://doi.org/10.3390/ijms222312752>
- [5] I. Bhat, S. Husain, W. Khan, S. Patil, *Materials Research Bulletin*. 48, 4506 (2013); <https://doi.org/10.1016/j.materresbull.2013.07.028>
- [6] L. Jia, M. D. Lloyd, M. R. Lees, L. Huang, R. I. Walton, *Inorg. Chem.* 62(11), 4503 (2023); <https://doi.org/10.1021/acs.inorgchem.2c04325>
- [7] S. Phokha, S. Hunpratup, S. Pinitsoontorn, B. Putasaeng, S. Rujirawat, S. Maensiri, *Materials Research Bulletin*, 67, 118 (2015); <https://doi.org/10.1016/j.materresbull.2015.03.008>
- [8] M. Mesbah, S. Hamedshahraki, S. Ahmadi, M. Sharifi, C. A. Igwegbe. *MethodsX*. 14(7), 100786 (2020); <https://doi.org/10.1016/j.mex.2020.100786>
- [9] S. Phokha, S. Pinitsoontorn, S. Maensiri, S. Rujirawat, *Journal of Sol-Gel Science and Technology*, 71, 333 (2014); <https://doi.org/10.1007/s10971-014-3383-8>
- [10] W. A. Shatti, Z. Mohammed Ali Abbas, Z. T. Khodair, *Journal of Ovonic Research*, 18(4), 473 (2022); <https://doi.org/10.15251/JOR.2022.184.473>
- [11] M. A. Ahmed, N. Okasha, M. M. El-Sayed, *Ceram. Int.* 33 (1), 49 (2007); <https://doi.org/10.1016/j.ceramint.2005.07.014>
- [12] N. Lwin, M. N. A. Fauzi, S. Sreekantan, R. Othman, *Physica B*. 461, 134 (2015); <https://doi.org/10.1016/j.physb.2015.01.001>
- [13] X. C. Zhong, X. J. Guo, S. Y. Zou, H. Y. Yu, Z. W. Liu, Y. F. Zhang, K. X. Wang, *AIP Advances*, 8, 047807 (2018); <https://doi.org/10.1063/1.4993645>
- [14] E. Grabowska, *Appl. Cat. B: Env.*, 186, 97 (2016); <https://doi.org/10.1016/j.apcatb.2015.12.035>
- [15] S. Acharya, J. Mondal, S. Ghosh, S. K. Roy, P. K. Chakrabarti, *Mat. Let.* 64, 415 (2010); <https://doi.org/10.1016/j.matlet.2009.11.037>
- [16] A. A. Sattar, H. M. El-Sayed, K. M. El-Shokrofy, M. M. El-Tabey, *J. Mat. Eng. Per.* 14, 99 (2005); <https://doi.org/10.1361/10599490522185>
- [17] Z. Peng, X. Fu, H. Ge, Z. Fu, C. Wang, L. Qi, *J. Magnetism and Magnetic Materials*. 323, 2513 (2011); <https://doi.org/10.1016/j.jmmm.2011.05.033>
- [18] M. S. Shifa, M. I. Khan, M. Mustaqeem, E. T. Munir, Z. A. Gilani, H. M. Noor Ul Huda Khan Asghar, M. S. Ahmed, I. Quresh. *Journal of Ovonic Research*, 17(1), 89 (2021).
- [19] T. J. Shinde, A. B. Gadkari, P. N. Vasambekar, *Journal of Alloys and Compounds*. 513, 80 (2012); <https://doi.org/10.1016/j.jallcom.2011.10.001>
- [20] M. Huq, D. Saha, R. Ahmed, Z. Mahmood, *Journal of Scientific Research*. 5, 215(2013); <https://doi.org/10.3329/jsr.v5i2.12434>
- [21] M. Schwartz, *Encyclopedia of Materials, Parts and Finishes*, CRC Press. 2(2002); <https://doi.org/10.1201/9781420017168>
- [22] G. Mustafa, I. Ahmed, M. U. Subhani, M. Shabaz, M. Iqbal, Enam-ul-Haq, S. Abbas, R. Mehmood, *Journal of Ovonic Research*, 17(3), 231 (2021); <https://doi.org/10.15251/JOR.2021.173.231>
- [23] G. Pecchi, P. Reyes, R. Zamora, C. Campos, L.E. Cadús, P. Bibiana, *Catalysis Today*, 133, 420 (2008); <https://doi.org/10.1016/j.cattod.2007.11.011>
- [24] X. Liu, B. Cheng, J. Hu, H. Qin, M. Jiang, *Sensors and Actuators B: Chemical*, 129, 53 (2008); <https://doi.org/10.1016/j.snb.2007.07.102>

- [25] A. Aizat, F. Aziz, M. N. Mohd Sokri, M. S. Sahimi, N. Yahya, J. Jaafar, A. F. Ismail, *Applied Sciences*. 1, 1(2019); <https://doi.org/10.1007/s42452-018-0104-x>
- [26] Q. Liu, Z. You, S. Zeng, H. Guo, J. Solgel. *Sci. Technol.* 80, 860 (2016); <https://doi.org/10.1007/s10971-016-4141-x>
- [27] L. J. Mao, C. Liu, *Mater. Res. Bull.* 43, 1384 (2008); <https://doi.org/10.1016/j.materresbull.2007.06.048>
- [28] P. Xiong, H. Huang, X. Wang, *Journal of Power Sources*. 245, 937 (2014); <https://doi.org/10.1016/j.jpowsour.2013.07.064>
- [29] K. Bindu, K. Sridharan, K. M. Ajith, H. N. Lim, H. S. Nagaraja, *Electrochim. Acta.* 17, 139 (2016); <https://doi.org/10.1016/j.electacta.2016.09.083>
- [30] M. M. Vadiyar, S. S. Kolekar, J. Y. Chang, A. A. Kashale, A. V. Ghule, *Electrochim. Acta.* 222, 1604 (2016); <https://doi.org/10.1016/j.electacta.2016.11.146>
- [31] L. Liu, H. Zhang, Y. Mu, Y. Bai, Y. Wang, *Journal of Power Sources*, 327, 599 (2016); <https://doi.org/10.1016/j.jpowsour.2016.07.104>
- [32] T. P. Gujar, W. Y. Kim, I. Puspitasari, K. D. Jung, O. S. Joo, *Int. J. Electrochem. Sci.* 2, 666 (2007); [https://doi.org/10.1016/S1452-3981\(23\)17102-1](https://doi.org/10.1016/S1452-3981(23)17102-1)
- [33] D. K. Pawar, S. M. Pawar, P. S. Patil, S. S. Kolekar, *J. Alloys Comp.* 509, 3587 (2011); <https://doi.org/10.1016/j.jallcom.2010.10.019>
- [34] W. Raza, G. Nabi, A. Shahzad, N. Malik, N. Raza, *J. Mat. Sci. Mat. Elect.* 32, 7443 (2021); <https://doi.org/10.1007/s10854-021-05457-w>